Nanoscale

Cite this: *Nanoscale*, 2012, **4**, 6532

www.rsc.org/nanoscale

PAPER

Investigation of ultraviolet optical properties of semiconducting-enriched and metal-enriched single-walled carbon nanotube networks using spectroscopic ellipsometry†

Young Ran Park,[a] Woo-Jae Kim,[b] Min Jae Ko,[c] Nam Ki Min[d] and Cheol Jin Lee*[a]

Received 17th May 2012, Accepted 15th August 2012
DOI: 10.1039/c2nr31205k

The ultraviolet optical properties of semiconducting-enriched and metallic-enriched single-walled carbon nanotube (semi-enriched and m-enriched SWCNT) networks were studied using spectroscopic ellipsometry. According to calculated energy loss function, the energy loss peak assigned to the maximum intensity of π-plasmon energy was found to increase from 4.5 eV to 5.0 eV as SWCNT network composition was changed from m-SWCNT enriched to semi-SWCNT enriched. These results clearly demonstrate that the dielectric response in the 4–6 eV range is sensitive to changes in the surrounding dielectric environment depending on the semi-/m-SWCNT content. Therefore, the spectral shift of this energy loss is attributed to the enhanced electron confinement by the presence of the surface plasmon due to a small amount of m-SWCNT, which is an important phenomenon at the SWCNT network.

1. Introduction

A single-walled carbon nanotube (SWCNT) is a rolled-up graphene in a cylindrical form. It is well known that the semiconducting or metallic property of SWCNT deeply depends on both diameter and chirality of SWCNT.[1–3] In a number of possible applications, including use of SWCNTs as field effect transistors,[4] conductive transparent thin films,[5] and field emission sources,[6] it is desirable to use SWCNT of only a single electronic type. However, synthesized SWCNTs are usually collected as bundles that contain both semiconducting- and metallic-SWCNT (semi- and m-SWCNT) with various chiralities.[7] For this reason, separation of semi- and m-SWCNT from SWCNT mixtures has been achieved by various techniques including density gradient centrifugation,[8–10] electrophoresis,[11] and gel chromatography.[12,13]

Most importantly, ultraviolet visible near-infrared (UV-vis-NIR) spectrometry is used to qualify the separation efficiency. The estimation of semi-/m-SWCNT ratio has proposed that areas of the S_{22} and M_{11} bands can be calculated using a linear fitting method,[14] allowing the proportion of semi- and m-SWCNTs to be estimated for the raw-SWCNTs. Since the absorption peaks at higher energy, including that regarded as the SWCNT π-plasmon, produced broad absorption baselines in the inter-subband region at lower energy, a sound understanding of their fundamental properties and physical origins are extremely important. So far, several theoretical and experimental studies have investigated UV absorption in SWCNTs.[15–19] However, the above mentioned linear fitting approach uses non-physical based linear subtraction at the peak minima. As a result, it is difficult to understand the relative electronic transitions of the SWCNTs, and the underlying absorption from the π-plasmon. Therefore, clear understanding of the UV absorption features is essential to fully utilize SWCNTs for various applications.

These absorption peaks have been observed in several studies of random oriented SWCNT films, but considerable disagreements are found among the discussion. In the previous reports, Murakami suggested that the observed peaks at 4.5 eV and 5.25 eV originate from the anisotropic optical properties of graphite, corresponding to the maxima in $\mathrm{Im}\{\varepsilon_{\perp}\}$ (parallel to the SWCNT axis) and $\mathrm{Im}\{-\varepsilon_{\parallel}^{-1}\}$ (perpendicular to the SWCNT axis), respectively,[15] and also showed that one of the two peaks in SWCNTs is a surface-plasmon or Mie resonance. It can be said that the Mie resonance still exists for bundled nanotubes.[17] Kataura *et al.* attributed the peak at 4.5 eV to π-plasmon absorption observed in a purified SWCNT film while 5.25 eV peak was only seen in the pristine sample containing amorphous carbon.[18] Pichler *et al.* stated from their electron energy loss spectroscopy (EELS) measurements on purified SWCNTs that the 5.2 eV peak observed a low electron momentum transfer was due to a π-plasmon along the SWCNT axis.[19]

[a]*School of Electrical Engineering, Korea University, Seoul 136-701, Republic of Korea. E-mail: cjlee@korea.ac.kr*
[b]*Department of Chemical and Environmental Engineering, Gachon University, Sungnam, Gyeonggi-do 461-701, Republic of Korea*
[c]*Photo-Electronic Hybrid Research Center, Korea Institute of Science and Technology, Hwarangno 14-gil 5, Seongbuk-gu, Seoul 136-791, Republic of Korea*
[d]*Department of Control and Instrumentation Engineering, Korea University, Chungnam 339-700, Republic of Korea*
† Electronic supplementary information (ESI) available. See DOI: 10.1039/c2nr31205k

In this work, we studied the effects of the electron confinement in semiconducting enriched and metal enriched (semi-enriched and m-enriched) SWCNT networks using spectroscopic ellipsometry (SE). In particular, we found that the energy loss peak exhibits remarkable and different behaviours depending on semi-/m-SWCNT content at SWCNT networks. Our results suggest that the electron confinement effect is significant because they influence the photon energy for the π-plasmon (related to the π–π* transition). This is a direct indication that the dielectric responses of the SWCNT networks have strong dependence on the surrounding dielectric environment.

2. Experimental section

We prepared arc-SWCNT random network films with different compositions of semi- and m-SWCNT using a simple vacuum filtration transfer method. Control of the ratio of semi-/m-SWCNT is adjusted by the agarose gel column chromatography method.[12,13]

To check the components of the unbound and bound fractions, the arc-SWCNT film, collected on a mixed cellulose ester membrane filter, was transferred onto a Corning glass substrate by a simple vacuum filtration transfer process. In order to determine the optoelectronic impact of oxygen adsorption on the surface of the SWCNT in prepared films, as-deposited SWCNT films were annealed by placing in vacuum at 200 °C and characterizing. It has previously been established that oxygen species adsorbed on the surface of SWCNT can act as hole dopants in SWCNT films.

The thicknesses of the SWCNT films were determined with field emission scanning electron microscopy and found to be in the range 230 ± 10 nm. High resolution grazing incident X-ray diffraction (HRGIXD) was measured by using HR-4 Crystal Triple Axis XRD (X' Pert-PRO/MRD). The optical absorbance was studied using a Cary 5000 UV-vis-NIR spectrometer at an incident angle (Φ) of 0° from the plane of incidence. Also a Woollam vacuum ultraviolet variable-angle spectroscopic ellipsometer (VUV-VASE) was used to measure the dielectric function of the separated SWCNTs network films at an incident angle (Φ) of 45° from the plane of incidence. SE measures the amplitude and the phase of ρ ($= r_p/r_s$), the complex reflectance ratio of the *p* (parallel) and *s* (perpendicular) field components of the light beam defined with respect to the plane of incidence of the sample.

3. Results and discussion

Fig. 1 shows the optical absorbance spectra for the separated SWCNT films over a wide energy range (0.5–6.0 eV) on an arbitrary coordinate axis. Due to the one dimensional (1D) electronic structure of SWCNT, 1D exciton absorption peaks associated with interband transitions between 1D Van Hove singularities E_{11} ($v_1 \rightarrow c_1$), E_{22}, and E_{33} of SWCNTs are observed.[21] The absorption peaks around 0.5–1.0 eV, 1.0–1.5 eV, and 2.3–2.8 eV are derived from first, second, and third (and forth) optical transition of semi-SWCNT, and are designated as S_{11}, S_{22}, and S_{33} (and S_{44}) respectively.[22] The absorbance peak around 1.5–2.3 eV and 2.8–3.5 eV represents the first and second optical transition of m-SWCNT (M_{11} and M_{22}), respectively. Separation of semi-enriched and m-enriched SWCNT was also confirmed by Raman spectroscopic analysis (see Fig. S1 and S2 in the ESI†).

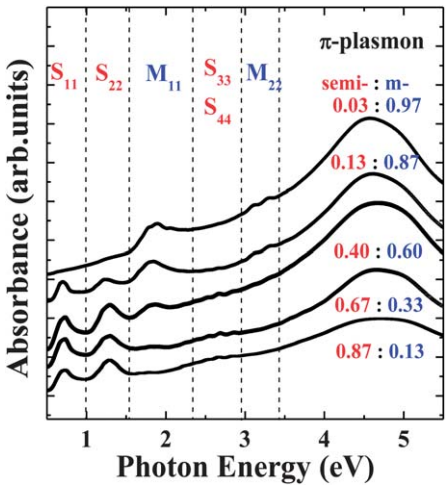

Fig. 1 UV-vis-NIR absorbance spectra for various separated SWCNT films. We estimated the actual composition from the relation between semi-/m-SWCNT area ratio (Fig. S3 and S4†) and extinction coefficient ratio ($k_m/k_{semi} = 0.352$).[20] Raw-SWCNT is 0.40 (semi)/0.60 (m).

In the previous works, the absorbance data were typically used to determine absorption in SWCNT materials.[14,15,17,18,20,22–24] But those approaches are not appropriate to observe the strong reflectance peak at the π-plasmon (see Fig. S5†). As shown in Fig. 1, the absorbance shows a broader peak at the π-plasmon resonance region compared with the interband transition region. To date, the bulk and surface plasmons in SWCNTs have mainly been studied using EELS, in which the energy loss peaks are attributed to π- and π + σ plasmon excitation. Especially, in the analysis of SE, the magnitude and the spectral shape of the complex dielectric function (see Fig. S6†) agree well with the energy portions of the spectrum derived from EELS data. The imaginary part of dielectric function, in the vanishing momentum transfer ($\boldsymbol{q}$) limit ($\boldsymbol{q} \rightarrow 0$), gives the optical absorption. Therefore, SE is very desirable to interpret the accurate analysis about the energy position of the π-plasmon.

Fig. 2 illustrates the calculated energy loss function $\{-\mathrm{Im}(1/\varepsilon(\boldsymbol{q},\boldsymbol{E}))\}$ from the dielectric function of SWCNT.[25,26] The strong peak at around 4.5–5.0 eV is the so-called π-plasmon, which is the collective excitation of the π-electron system at SWCNT. In contrast to the absorbance data (Fig. 1), the energy loss function (Fig. 2(a)–(e)) presents the different energy loss peaks in the range of 4.5–5.0 eV and reveals one-fold plasmon dispersion. In addition, Fig. 2(f) shows the semi-SWCNT (95% purity) network film of Nanointegris Inc. It is seen that the energy loss peak of SWCNT shifts to higher energies with the increase of the semi-SWCNT content. That is, a feature at 4.5 eV reveals dominantly m-enriched SWCNT while that at 5.0 eV indicates mainly semi-enriched SWCNT.

To investigate the impact of the bundling on the π-plasmon spectrum, we carried out the grazing incidence with high resolution grazing incidence X-ray diffraction (HRGIXD)

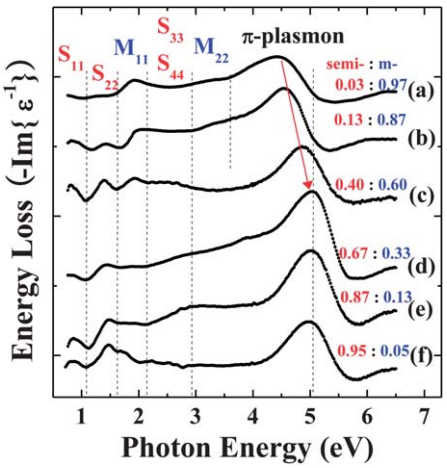

Fig. 2 Calculated energy loss function *vs.* photon energy plots of semi- and m-SWCNTs compared with that of raw-SWCNTs. π-plasmon energy shifts from 5.0 eV to 4.5 eV as SWCNT network was changed from semi-SWCNT to m-SWCNT. (f) is semi-SWCNT (95% purity) network film of Nanointegris Inc.

experiments using the Kα emission of a Cu anode at room temperature. A highly bundled sample would have a significantly different dielectric constant and level of intertube interactions to one with a lower degree of bundling, even if the two samples were to have a similar degree of percolation pathways.[27,28] Fig. 3 shows the in-plane ($\psi = 90°$) XRD patterns of the θ–2ω scans obtained for HRGIXD. As shown in Fig. 3, there is no indication of the bundle peak expected at low momentum transfer in all SWCNT films. The broad hump between 1 and 2 $Å^{-1}$ may be due to the amorphous distribution of the glass substrate present in the sample. The bundled degree of semi-enriched and m-enriched SWCNT was also confirmed by field emission scanning electron microscopy analysis (see Fig. S7 in the ESI†).

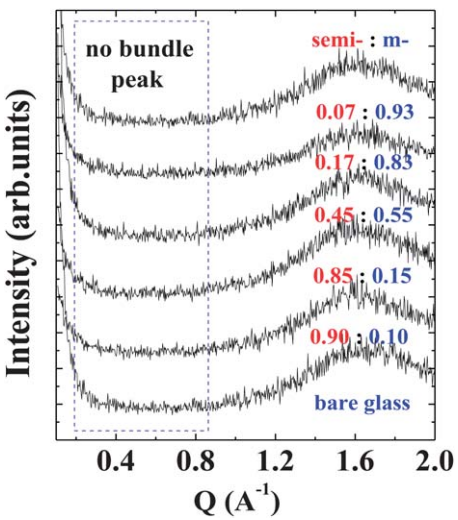

Fig. 3 The X-ray diffraction patterns of the raw-, semi-enriched, and m-enriched SWCNT network films. The inset shows the first bundle diffraction region with increasing semi-SWCNT content (but no bundle peak in the low-q region).

In Fig. 1, due to an arbitrary ordinate axis, we can explain that the broad UV absorption peak in the 4–6 eV range actually consists of two distinct components. In particular, the absorption feature at 4.5 eV is observed for light polarized parallel to the SWCNT axis, while the other absorption feature at 5.0 eV is observed for light polarized perpendicular to the axis.

We described a Lorentzian curve fitting from the experimental results as shown in Fig. 4(a). The magnitude ratio of $I_{(5.0\ eV)}/I_{(4.5\ eV)}$, $I_{(4.0\ eV)}/I_{(4.5\ eV)}$, and $I_{(2.8\ eV)}/I_{(4.5\ eV)}$ plotted against the semi-SWCNT ratio was obtained by the Lorentz decomposition of corresponding optical absorbance spectra (see Fig. S3†). Their widths were fixed at 4.0, 1.3, 0.98, and 1.72 eV. It is seen that the magnitude ratio of $I_{(5.0\ eV)}/I_{(4.5\ eV)}$ is dramatically enhanced with the increase of the semi-SWCNT ratio. This result demonstrated that the characteristic absorption peaks near 5 eV can be affected by the dielectric environment, which depends on the semi-/m-SWCNT content. The significant enhancement of this absorption is explained by the much larger dielectric response of semi-SWCNT than of air. In 1D metallic nanowire, we note that the direction perpendicular to the nanowire axis (the direction of electron confinement) is the direction in which dipolar surface plasmons (DSP) can be excited. Therefore, changes observed in the fitting intensity ratio of 4.5 and 5.0 eV are well explained in terms of the enhanced electron confinement from the DSP.

Fig. 4(b) shows the π-plasmon energy shifts estimated by the energy loss function (Fig. 2) of the SWCNT film calculated from the SE *vs.* semi-SWCNT ratio. In any case, our results clearly show that the energy loss function of SWCNTs at around 4.5–5.0 eV is dependent on semi-/m-SWCNT content at SWCNT networks.

Fig. 5 shows an illustration of the p (parallel) and s (perpendicular) field components of the light beam defined with respect to the plane of incidence of the SWCNT network film. SE data indicate that there should be a significant reflection in the spectral region associated with the π-plasmon. At low angles of incidence, both p- and s-polarized lights are in the plane of the SWCNT network, likely contributing to the relatively small reflectance with the π-plasmon at normal angle for both polarizations, and then deviating strongly at high angles due to the screening effect (see Fig. S5†). This dependence of the calculated reflectance data on the high incident light polarization confirms

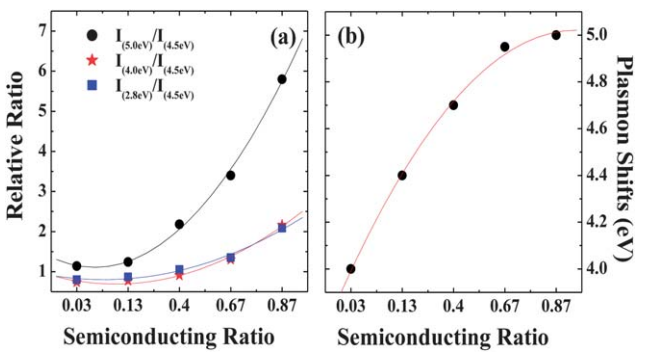

Fig. 4 (a) The ratio of magnitudes of Lorentzian-fitted curves at $I_{(5.0\ eV)}/I_{(4.5\ eV)}$, $I_{(4.0\ eV)}/I_{(4.5\ eV)}$, and $I_{(2.8\ eV)}/I_{(4.5\ eV)}$, (b) π-plasmon energy shifts, according to semi-SWCNT ratio (black, blue, and red lines are fitting curves).

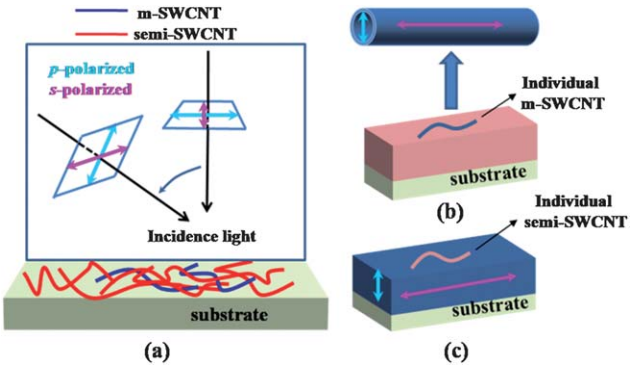

Fig. 5 Illustration of the incidence light at the sample surface. (a) The *p* (parallel) and *s* (perpendicular) field components of the light beam defined with respect to the plane of incidence of the SWCNT network film; (b) semi-enriched SWCNT network film, and (c) m-enriched SWCNT network film.

that surface plasmons (SPs) are generated with *p*-polarized light, since all the electric and magnetic components for *s*-polarized light are continuous across the interface (between upper and lower SWCNT) according to Maxwell's boundary conditions. Therefore, no surface charge density will be induced for *s*-polarized light to form collectively oscillating SPs.

The photon energy corresponding to the maximum SP excitation depends on both the dielectric constant and the charge density of the material. There are several reasons, such as strong SWCNT network interactions, which cannot be described by excitonic effects, different levels of anisotropy in different samples, the reduction of the π-bond strength due to disorder, or dipole–dipole level. Thus, these interactions could lead to the observed trend of π-plasmon energy. It implies that the dielectric function of the SWCNT film is determined by the density of the SWCNT only, while the dielectric response of the individual SWCNT would be the same in isolated SWCNT.

As shown in Fig. 5(b) and (c), the electron confinement effect of the individual m-SWCNT is expected to dominate, and that of the m-enriched SWCNT film is released due to variable connectivity in the network, which is explained by the fact that the metallic behavior in a SWCNT network arises when the m-SWCNT network is percolating. Thus, the energy upshifting with the increase of semi-SWCNT content suggests that dielectric response depends on the degree of electron confinement by the presence of the SPs. In the m-enriched SWCNT network, the electron confinement effects are reduced due to a highly connected m-SWCNT network, which removes the absorption peak around 5.0 eV. On the other hand, in the semi-enriched SWCNT network, a significant shift of this absorption is explained by the fact that the electron confinement is enhanced by the reduction of a percolation. It is known that the percolation path between m- and semi-SWCNT interconnects has been shown to be less than the percolation path between m- and m-SWCNT junctions. A decrease in the amount of m-SWCNT to enhance electron confinement can result in greater energy losses from electron–surface collisions that reduced the mean free path of apparent electrons. The π-plasmon shift was more apparent when the content of semi-SWCNTs was smaller than 0.5 whereas little change was observed when it was greater than 0.67. There is considered to be a more rapid change in shift at m-enriched SWCNTs considering the percolation of m-SWCNTs at relatively high concentrations. In contrast, we estimated that a small change in shift at semi-enriched SWCNTs could be caused by a unique tubular structure (and also a similar range of about 1.2 nm diameter) between isolated m-SWCNTs. Metal nanostructures can be fabricated in various sizes and shapes.[29] Compared with metal nanostructures, m-SWCNTs have limited size and the shape. As a result, plasmon resonance peaks of SWCNT films are a little increased at a semi-enriched SWCNT region. Thus, in the semi-enriched SWCNT network, the probability of all m-SWCNT paths is low, so that electron confinement is enhanced. Also, it is due to the charge density oscillation and confinement between the metallic nanostructures; the features strongly depend on a nanostructure's composition, size, shape, inter-nanostructure distance, and local dielectric environment.[30,31]

Thus, we consider that the result of the spectral shift at the UV region as shown in Fig. 4(b) is caused by the electron confinement effects due to the change of the dielectric environments depending on the semi-/m-SWCNT content in the random network of SWCNTs.

4. Conclusions

We investigated the effects of the electron confinement in semi-enriched and m-enriched SWCNT network. The calculated energy losses show that the π-plasmon peak of SWCNTs shifts to higher energies with increasing semi-SWCNT content. This phenomenon is attributed to the enhanced electron confinement at semi-enriched SWCNT network. We suggest that the improvement of the optical properties in semiconducting materials using the electron confinement effect open pathways for applying SWCNT to various potential applications in highly efficient optoelectronic devices.

Acknowledgements

This work was supported by the World Class University Project (WCU, R32-2010-000-10082-0) funded by the Ministry of Education, Science, and Technology, New & Renewable Energy of the Korea Institute of Energy Technology Evaluation and Planning (KETEP) grant funded (no. 2010T100100651) by the Korea government Ministry of Knowledge Economy, National Research Foundation of Korea (NRF) grant funded by the Korea Government (MEST) (K20903001812-11E0100-01700), and Basic Science Research Program through the National Research Foundation of Korea (NRF) funded by the Ministry of Education, Science and Technology (2011-0005392).

Notes and references

1 R. Saito, M. Fujita, G. Dresselhaus and M. S. Dresselhaus, *Phys. Rev. B: Condens. Matter*, 1992, **46**, 1804–1811.
2 J.-C. Charlier and R. H. Lambin, *Phys. Rev. B: Condens. Matter*, 1998, **57**, R15037–R15039.
3 C. T. White and T. N. Todorv, *Nature*, 1991, **393**, 240–242.
4 M. Engel, J. P. Small, M. Steiner, M. Freitag, A. A. Green, M. C. Hersam and P. Avouris, *ACS Nano*, 2008, **2**, 2445–2452.
5 A. A. Green and M. C. Hersam, *Nano Lett.*, 2008, **8**, 1417–1422.
6 S.-I. Jung, J. S. Choi, H. C. Shim, S. Kim, S. H. Jo and C. J. Lee, *Appl. Phys. Lett.*, 2006, **89**, 233108.

7 P. M. Ajayan, *Chem. Rev.*, 1999, **99**, 1787–1800.
8 M. S. Arnold, A. A. Green, J. F. Hulvat, S. I. Stupp and M. C. Hersam, *Nat. Nanotechnol.*, 2006, **1**, 60–65.
9 S. Ghosh, S. M. Bachilo and R. B. Weisman, *Nat. Nanotechnol.*, 2010, **5**, 443–450.
10 W.-J. Kim, N. Nair, C. Y. Lee and M. S. Strano, *J. Phys. Chem. C*, 2008, **112**, 7326–7330.
11 T. Tanaka, H. H. Jin, Y. Miyata and H. Kataura, *Appl. Phys. Express*, 2008, **1**, 114001.
12 T. Tanaka, Y. Urabe, D. Nishide and H. Kataura, *Appl. Phys. Express*, 2009, **2**, 125002.
13 H. Liu, D. Nishide, T. Tanaka and H. Kataura, *Nat. Commun.*, 2011, **2**, 309.
14 M. E. Itkis, D. E. Perea, S. Niyogi, S. M. Rickard, M. A. Hamon, H. Hu, B. Zhao and R. C. Haddon, *Nano Lett.*, 2003, **3**, 309–314.
15 Y. Murakami, E. Einarsson, T. Edamura and S. Maruyama, *Phys. Rev. Lett.*, 2005, **94**, 087402.
16 T. McNeish, G. Gumbs and A. Balassis, *Phys. Rev. B: Condens. Matter Mater. Phys.*, 2008, **77**, 235440.
17 Y. Murakami and S. B. Maruyama, *Phys. Rev. B: Condens. Matter Mater. Phys.*, 2009, **79**, 155445.
18 H. Kataura, Y. Kumazawa, Y. Maniwa, I. Umezu, S. Suzuki, Y. Ohtsuka and Y. Achiba, *Synth. Met.*, 1999, **103**, 2555–2558.
19 T. Pichler, M. Knupfer, M. S. Golden, J. Fink, A. Rinzler and R. E. Smally, *Phys. Rev. Lett.*, 1998, **80**, 4729.
20 W. J. Kim, C. Y. Lee, K. P. O'brien, J. J. Plombon, J. M. Blackwell and M. S. Strano, *J. Am. Chem. Soc.*, 2009, **131**, 3128–3129.
21 M. S. Strano, *J. Am. Chem. Soc.*, 2003, **125**, 16148–16153.
22 K. K. Kim, J. J. Bae, H. K. Park, S. M. Kim, H. Z. Geng, K. A. Park, H. J. Shin, S. M. Yoon, A. Benayad, J. Y. Choi and Y. H. Lee, *J. Am. Chem. Soc.*, 2008, **130**, 12757–12761.
23 A. V. Naumov, S. Ghosh, D. A. Tsyboulski, S. M. Bachilo and R. B. Weisman, *ACS Nano*, 2011, **5**, 1639–1648.
24 J. A. Fagan, J. R. Simpson, B. J. Bauer, S. H. P. Lacerda, M. L. Becker, J. Chun, K. B. Migler, A. R. H. Walker and E. K. Hobbie, *J. Am. Chem. Soc.*, 2007, **129**, 10607–10612.
25 H. Ehrenreich and M. H. Cohen, *Phys. Rev.*, 1959, **115**, 786–790.
26 M. F. Lin, D. S. Chuu, C. S. Huang, Y. K. Lin and K. W.-K. Shung, *Phys. Rev. B: Condens. Matter*, 1996, **53**, 15493–15496.
27 E. Einarsson, H. Shiozawa, C. Kramberger, M. H. Rummeli, A. Gruneis, T. Pichler and S. Maruyama, *J. Phys. Chem. C*, 2007, **111**, 17861–17864.
28 X. Liu, T. Pichler, M. Knupfer, M. S. Golden, J. Fink, D. A. Walters, M. J. Casavant, J. Schmidt and R. E. Smalley, *Synth. Met.*, 2001, **121**, 1183–1186.
29 Y.-J. Wu, C.-H. Hsieh, P.-H. Chen, J.-Y. Li, L.-J. Chou and L.-J. Chen, *ACS Nano*, 2010, **4**, 1393–1398.
30 A. G. Van der Geest, K. E. Hurst, N. D. Bronstein, J. H. Lehman and M. T. Lusk, *Phys. Rev. B: Condens. Matter Mater. Phys.*, 2010, **81**, 115440.
31 S. Link and M. A. El-Sayed, *J. Phys. Chem. B*, 1999, **103**, 8410–8426.